Ru, Rh and Ir metal complexes of pyridyl chalcone derivatives: Their potent antibacterial activity, comparable cytotoxicity potency and selectivity to cisplatin

Lincoln Dkhar[a], Venkanna Banothu[b], Emma Pinder[c], Roger M. Phillips[c], Werner Kaminsky[d], Mohan Rao Kollipara[a]*

[a]Centre for Advanced Studies in Chemistry, North-Eastern Hill University, Shillong 793 022, India.

[b]Centre for Biotechnology (CBT), Institute of Science & Technology (IST), Jawaharlal Nehru Technological University Hyderabad (JNTUH), Kukatpally-500 085, Hyderabad, Telangana State, India.

[c]Department of Pharmacy, School of Applied Sciences, University of Huddersfield, Huddersfield, HD1 3DH UK.

[d]Department of Chemistry, University of Washington, Seattle, WA 98195, USA

E mail: mohanrao59@gmail.com

Abstract

Half sandwich ruthenium, rhodium and iridium complexes containing pyridyl chalcone analogues (**L1** and **L2**) are prepared by the reaction of $[(arene)M(\mu\text{-}Cl)Cl]_2$ (arene = benzene, *p*-cymene, Cp*) and (M =Ru, Rh/Ir)] with **L1** and **L2** in 1:2 (M:L) ratio. Eight neutral mononuclear complexes (**1-8**) were obtained and characterized using FT-IR, ^{1}H-NMR, ^{13}C-NMR, ESI mass and UV-Vis spectroscopic methods. The molecular structures of complexes **2**, **4**, **5** and **7** are established by single crystal X-ray diffraction studies. Antibacterial studies were tested against three strains of bacterial microorganisms *Staphylococcus aureus* (gram +*ve*), *Klebsiella pneumoniae* (gram -*ve*) and *Escherichia coli* (gram -*ve*). Further the cytotoxicity study of the pyridyl chalcone derivatives and their complexes were evaluated against the human colorectal cancer cell lines HT-29, HCT-116 $p53^{+/+}$, HCT-116 $p53^{-/-}$ and ARPE-19 (non-cancer retinal epithelium).

Keywords: ruthenium, rhodium, iridium, pyridyl chalcone, antibacterial, anticancer

1. Introduction

Cancer is one of the major causes of death in both developed and developing countries [1]. Although the availability of drugs has increased over recent years, mortality rates remain high and long-term responses are thwarted by problems of toxicity and the emergence of resistance [2]. In recent years, there has been a resurgence interest in organometallic complexes that have different modes of action compared to the platinates [3]. In our quest to find more effective treatments for cancer, other metal-based compounds incorporating ruthenium, rhodium and iridium have been developed and these have shown promising activity [4]. High selectivity of ruthenium complexes towards cancer cells rather than healthy cells and their stable oxidation states under bodily conditions showed that they are promising antitumor agents [5]. The biological activity of the metal complexes of ruthenium, rhodium and iridium can be a consequence of the coordination or intercalation mode of binding to the DNA [6]. Some of the arene ruthenium complexes prepared by Sadler *et al.* showed promising anticancer activity both in *vitro* and in *vivo* [7]. The anticancer activities of arene ruthenium complexes can be enhanced based on the ligand scaffolds, which play an important role in controlling their activity such as improving their water solubility. For example, bioactive compounds such as flavonoids, isoflavonoids *etc.,* can be incorporated to arene Ru(II) complexes to enhance their anticancer activities [8]. Also, bioactive ligand scaffolds such as chalcone when combined with these arene metal complexes exhibit better anticancer activity [9].

The wide range of biological activities associated with chalcone based compounds, both natural and synthetic, their ease of preparation, the potential of oral administration, safety and profound natural abundance have led us to explore their therapeutic potential when combined with metal complexes. Present-day studies have identified different chalcones and their hybrids as the active component for anticancer and antibacterial activity. The increasing incidence of infection caused by the rapid development of bacterial resistance to most of the known antibiotics is a serious health problem [10]. Thus, research efforts for finding effective nature-derived therapeutics against these multidrug-resistant microbes are required. Mai et al. have reported a series of chalcone derivatives where -NH_2 group on ring A (Chart 1) play an important role in the anti-proliferative effect against HT-29 cancer cell [11]. However, in this work, ring A contains either -NH_2 group or -OH group and ring B is replaced with pyridyl substituent.

Keeping in mind the anti-proliferative effect of -NH_2 substituent on ring A of chalcone derivatives we are interested to explore this possibility by complexing pyridyl chalcone derivatives (Chart 1) with arene ruthenium, rhodium and iridium complexes. The initial studies designed to assess their cytotoxic potency against cancer and non-cancer cells are described. Because of the reported activity of chalcones against microbes, the activity of these complexes against bacterial strains is also reported.

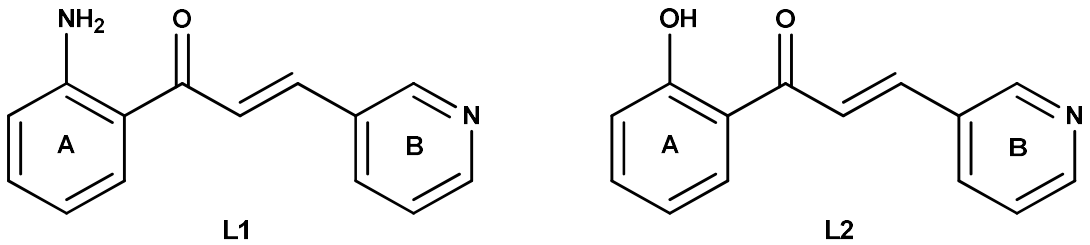

Chart 1: Ligands used in this study

2. Experimental Section

2.1 Physical methods and materials

All the reagents were purchased from commercial sources and used as received. 3-aminopyridine, 2-aminoacetophenone, 2-hydroxyacetophenone were obtained from Aldrich. The solvents were purified and dried according to standard procedures. The starting precursor metal complexes $[Cp^*MCl_2]_2$ (M = Rh/Ir) were prepared by a new procedure using Anton Paar Monowave 50 synthesis reactor. Infrared spectra were recorded on a Perkin-Elmer 983 spectrophotometer by using KBr pellets in the range of 400-4000 cm^{-1}. ^1H NMR spectra were recorded on a Bruker Avance II 400 MHz spectrometer using DMSO-d_6 and $CDCl_3$ as solvents. Absorption spectra were recorded on a Perkin-Elmer Lambda 25 UV/Visible spectrophotometer in the range of 200-800 nm at room temperature in acetonitrile. Mass spectra were recorded using Q-T of APCI-MS instrument (model HAB 273). Perkin-Elmer 2400 CHN/S analyzer was used for elemental analyses of the complexes. All these mononuclear metal complexes were synthesized and characterized by using FT-IR, ^1H NMR, ^{13}C-NMR, ESI mass, CHN, UV-Vis, and Single-crystal X-ray diffraction techniques.

2.2 Single-crystal X-ray structures analyses

Single crystal X-ray diffraction data for the complexes (**2**), (**4**), (**5**) and (**7**) were collected on an Oxford Diffraction Xcalibur Eos Gemini diffractometer at 293 K using graphite monochromated Mo-Kα radiation (λ = 0.71073 Å). Suitable crystals were selected and each

mounted on a glass fiber. The strategy for the data collection was evaluated using the CrysAlisPro CCD software [12]. Crystal data were collected by standard ''phi–omega scan'' techniques and were scaled and reduced using CrysAlisPro RED software. The structures were solved by direct methods using SHELXS-97 and refined by full-matrix least-squares with SHELXL-97 refining on F^2 [13, 14]. The positions of all the atoms were obtained by direct methods. Metal atoms in the complex were located from the E-maps and non-hydrogen atoms were refined anisotropically. The hydrogen atoms bound to the carbon were placed in geometrically constrained positions and refined with isotropic temperature factors, generally 1.2 U_{eq} of their parent atoms. Figure 1 was drawn with the ORTEP3 program [15]. Figures 2-5 were drawn with the MERCURY3.6 program [16].

2.3 Cell lines testing, culture condition and cytotoxicity studies

The *in vitro* cytotoxicity of the pyridyl chalcone ligands (**L1** and **L2**) and their corresponding arene d^6 metal complexes were performed at the University of Huddersfield against the HCT-116 $p53^{+/+}$, HCT-116 $p53^{-/-}$ and HT-29 human colorectal cancer lines. To compare the activity of complexes against cancer cells compared to non-cancer cells, complexes were also evaluated against the retinal epithelium cell line ARPE-19. HT-29 and ARPE-19 cells were originally purchased from ATCC and HCT-116 cells (containing wild type p53 or deleted p53) were obtained from Professor Bert Vogelstein's laboratory [17]. All reagents used were purchased from Sigma Aldrich Co. Ltd (Dorset, UK) unless otherwise stated. Antiproliferative activity of the compounds was evaluated using the standard MTT (3-(4,5-dimethylthiazol-2-yl)-2,5-diphenyltetrazolium bromide) cellular viability assay as described elsewhere [18]. Briefly, cells were seeded into 96 well plates of 1.5 x 10^3 cells per well and incubated for 24 hours at 37ºC in an atmosphere of 5% CO_2 before drug exposure. Generally, a stock solution was freshly prepared by dissolving each of the compounds in DMSO at a concentration of 100 mM. The highest concentration of drug tested was 100µM and the final DMSO concentration applied to cells was 0.1% (*v*/*v*), which is nontoxic to cells. Cisplatin was dissolved in phosphate-buffered saline at a stock concentration of 25 mM. The cells were exposed to a range of drug concentrations for 96 hours and cell survival was determined using the MTT assay [18, 19]. Following drug exposure, 20 µL of MTT (0.5 mg/mL) in phosphate-buffered saline was added to each well and it was further incubated at 37 °C for 4 hours in an atmosphere containing 5% CO_2. The solution was then removed and the formed formazan crystals were dissolved in 150 µM

DMSO. The absorbance of the resulting solution was recorded at 550 nm using an ELISA spectrophotometer. The percentage of cell survival was calculated by dividing the true absorbance of the treated cell by the true absorbance for controls (exposed to 0.1% DMSO). The IC_{50} values presented in Table 1 were determined from plots of percentage survival against drug concentration. Each experiment was performed in triplicate and a mean value obtained and stated as IC_{50} (μM) ± SD. To compare the response of non-cancer cells to cancer cells, the selectivity index (SI) presented in Table 2 was also calculated which is defined as the IC_{50} for ARPE 19 cells divided by the IC_{50} for each cancer cell line. Values >1 indicate that complexes have selective activity against cancer compared to non-cancer cells *in vitro*.

2.4 In vitro antimicrobial evaluation

All the Gram-negative and Gram-positive bacterial strains used for the present study were obtained from the Department of Microbiology, Osmania General Hospital, Hyderabad. All strains were tested for purity by standard microbiological methods. The bacterial stock cultures were maintained on Mueller-Hinton agar slants and stored at 4˚C. An agar-well diffusion method [20] was employed for the evaluation of antibacterial activities of test compounds. DMSO was used as a negative control. The bacterial strains were reactivated from stock cultures by transferring into Mueller-Hinton broth and incubating at 37 ˚C for 18 h. A final inoculum containing 10^6 colonies forming units (1 x 10^6 CFU/mL) was added aseptically to MHA medium and poured into sterile petri dishes. Different test compounds at a concentration of 200 µg per well were added to wells (8 mm in diameter) punched on an agar surface. Plates were incubated overnight at 37 ºC and the diameter of inhibition zone (DIZ) around each well was measured in mm. Experiments were performed in triplicates and these data were presented in Table 3.

The minimum inhibitory concentration (MIC) and minimum bactericidal concentration (MBC) was determined by the micro-broth dilution method done in 96 well plates according to the standard protocol [21]. A 2-fold serial dilution of the compounds, with the appropriate antibiotic, was prepared. Initially, 100 µl of MH broth was added to each well plate. Then 100 µl of compound or antibiotic was taken from the stock solution and dissolved in the first well plate. Serial dilution was done to obtain different concentrations. The stock concentrations of 2.0 mg/ml 24 hours culture turbidity was adjusted to match 0.5 McFarland standards which correspond to 1×10^8 CFU/ml. The standardized suspension (100 µl) of bacteria was added to all the wells except the antibiotic control well and the 96 well plates were incubated at 37 °C for 24

h. After 24 h of incubation 40 µl of MTT (3-(4,5-dimethlthiazol-2-yl)-2,5-diphenyltrazolium bromide) reagent (0.1 mg/ml in 1x PBS) was added to all the wells. MIC was taken as the lowest concentration which did not show any growth which was visually noted from the blue color developed by MTT. Subcultures were made from clear wells and the lowest concentration that yielded no growth after subculturing was taken as the MBC. The MIC and MBC values of tested compounds were presented in Table 4.

2.5 Synthesis of rhodium and iridium dimer

In a sample test tube of size 10 ml 500 mg of $RhCl_3/IrCl_3.nH_2O$, 0.4 ml of Cp* and 3 ml of dry methanol were added and mix thoroughly. A small size Teflon coated magnetic stirrer was inserted for stirring purpose. The mixture was sealed tightly and placed into an Anton Paar Monowave 50 synthesis reactor. The reaction condition was adjusted by setting the temperature to 110 °C and pressure will reach around 20 bars over 45 minutes. The instrument takes about 2-3 minutes to heat up to the set temperature and the reaction proceeds smoothly for 45 minutes. On completion, the reaction cools down to a temperature of 60 °C. A red-orange crystalline solid was obtained. The solvent was decanted, washed three times with diethyl ether and air-dried.

Yield: 87% for Rhodium dimer and 90% for Iridium dimer

*2.6 General procedure for the synthesis of metal complexes (**1-8**)*

To a solution of metal precursor $[(arene)MCl_2]_2$ (arene = p-cymene / benzene) and $[Cp^*MCl_2]_2$ (M = Rh/Ir) complexes (0.1 mmol), pyridyl chalcone analogue (**L1** and **L2**) (0.2 mmol) were added and stirred at room temperature in dry methanol (10 ml) for 5 hours (Scheme 1). The product starts to precipitate after 4 hours of stirring and was allowed to stir for another one hour for the overall conversion of the reactant into the desired product. The solid precipitate was centrifuged, washed thoroughly with diethyl ether and air-dried.

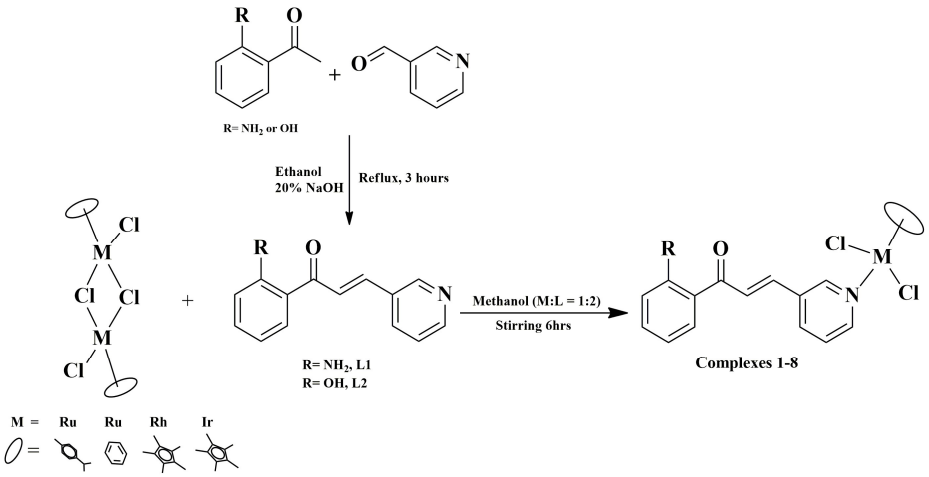

Scheme 1: Schematic representation for the synthesis of ligands and complexes **1-8**

2.6.1 [(p-cymene)Ru($\kappa^1_{(N)}$-L1)Cl_2] (1)

Color: Yellow; Yield: 81%; FT-IR (KBr, cm^{-1}): 3406 (υ_{N-H}), 3291 (υ_{N-H}), 1651 ($\upsilon_{C=O}$), 1616-1584 ($\upsilon_{C=N}$); ^{1}H NMR (400 MHz, DMSO-d_6) δ 9.07 (d, J = 4 Hz, 1H), 8.68 (d, J = 4 Hz, 1H), 8.43 (d, J = 8 Hz, 1H), 8.21 – 8.17 (m, 2H), 7.74 (d, J = 16 Hz, 1H), 7.57 (dd, J = 4, 4 Hz, 1H), 7.38 (t, J = 8 Hz, 1H), 6.89 (d, J = 8 Hz, 1H), 6.68 (t, J = 8 Hz, 1H), 5.91 (d, J = 4 Hz, 2H), 5.87 (d, J = 4 Hz, 2H), 2.91 (sept, 1H), 2.17 (s, 3H), 1.27 (d, J = 8 Hz, 6H); ESI-MS (m/z): 459.21 $[M\text{-}Cl]^+$-HCl; UV-Vis {Acetonitrile, λ_{max} nm ($\varepsilon/10^{-4}$ M^{-1} cm^{-1})}: 239 (4.896), 292 (5.588), 401 (2.013).

2.6.2 [(benzene)Ru($\kappa^1_{(N)}$-L1)Cl_2] (2)

Color: Yellow; Yield: 78%; FT-IR (KBr, cm^{-1}): 3421 (υ_{N-H}), 3312 (υ_{N-H}), 1650 ($\upsilon_{C=O}$), 1615-1589 ($\upsilon_{C=N}$); ^{1}H NMR (400 MHz, DMSO-d_6): δ 9.23 (s, 1H), 8.73 (d, J = 8 Hz, 2H), 8.23 (d, J = 16 Hz, 1H), 8.12 (d, J = 8 Hz, 1H), 7.83 (t, J = 8 Hz, 1H), 7.69 (d, J = 16 Hz, 1H), 7.30 (t, J = 8 Hz, 1H), 6.81 (d, J = 8 Hz, 1H), 6.59 (t, J = 8 Hz, 1H), 5.95 (s, 6H); ^{13}C NMR (100 MHz, DMSO-d_6): δ = 189.6, 152.1, 144.7, 144.4, 140.7, 136.0, 134.7, 131.5, 127.7, 116.9, 114.5, 87.5; ESI-MS (m/z): 403.03 $[M\text{-}Cl]^+$-HCl; UV-Vis {Acetonitrile, λ_{max} nm ($\varepsilon/10^{-4}$ M^{-1} cm^{-1})}: 240 (3.285), 291 (3.806), 402 (1.359).

2.6.3 [Cp*Rh($\kappa^1_{(N)}$-L1)Cl_2] (3)

Color: Orange; Yield: 85%; FT-IR (KBr, cm^{-1}): 3423 (υ_{N-H}), 3308 (υ_{N-H}), 1652 ($\upsilon_{C=O}$), 1615-1584 ($\upsilon_{C=N}$); ^{1}H NMR (400 MHz, DMSO-d_6) δ 8.92 (s, 1H), 8.49 (d, J = 4 Hz, 1H), 8.39 (d, J = 8 Hz, 1H), 7.97 (d, J = 16 Hz, 1H), 7.90 (d, J = 8 Hz, 1H), 7.50 (d, J = 8 Hz, 1H), 7.46 (d, J = 16 Hz, 1H), 7.09 (t, J = 8 Hz, 1H), 1.40 (s, 15H); ESI-MS (m/z): 461.24 $[M\text{-}Cl]^+$-HCl; UV-Vis {Acetonitrile, λ_{max} nm ($\varepsilon/10^{-4}$ M-1 cm-1)}: 233 (4.831), 283 (3.675), 402 (1.540).

2.6.4 [Cp*Ir($\kappa^1_{(N)}$-L1)Cl_2] (4)

Color: Yellow; Yield: 83%; FT-IR (KBr, cm^{-1}): 3430 (υ_{N-H}), 3312 (υ_{N-H}), 1652 ($\upsilon_{C=O}$), 1615-1583 ($\upsilon_{C=N}$); ^{1}H NMR (400 MHz, DMSO-d_6) δ 9.00 (s, 1H), 8.60 (d, *J* = 4 Hz, 1H), 8.37 (d, *J* = 8 Hz, 1H), 8.12-8.08 (m, 2H), 7.64 (d, *J* = 16 Hz, 1H), 7.50 (dd, *J* = 4, 4 Hz, 1H), 7.28 (t, *J* = 8 Hz, 1H), 6.80 (d, *J* = 12 Hz, 1H), 6.58 (t, *J* = 8 Hz, 1H), 1.62 (s, 15H); ^{13}C NMR (100 MHz, DMSO-d_6 + $CDCl_3$): δ = 198.75, 150.43, 134.00, 130.36, 124.51, 116.92, 114.89, 92.16, 85.18, 8.17; ESI-MS (m/z): 551.30 $[M-Cl]^+$-HCl; UV-Vis {Acetonitrile, λ_{max} nm ($\varepsilon/10^{-4}$ M^{-1} cm^{-1})}: 235 (3.212), 290 (3.532), 398 (1.157).

2.6.5 [(p-cymene)Ru($\kappa^1_{(N)}$-L2)Cl_2] (5)

Color: Yellow; Yield: 86%; FT-IR (KBr, cm^{-1}): 3447 (υ_{O-H}), 1637 ($\upsilon_{C=O}$), 1607-1581 ($\upsilon_{C=N}$); ^{1}H NMR (400 MHz, DMSO-d_6) δ 12.48 (s, 1H), 9.14 (s, 1H), 8.72 (d, *J* = 4 Hz, 1H), 8.47 (d, *J* = 8 Hz, 1H), 8.35 (d, *J* = 8 Hz, 1H), 8.26 (d, *J* = 16 Hz, 1H), 7.95 (d, *J* = 16 Hz, 1H), 7.68 (t, *J* = 8 Hz, 1H), 7.61 (t, *J* = 8 Hz, 1H), 7.13-7.10 (m, 2H), 5.91 (d, *J* = 4 Hz, 2H), 5.87 (d, *J* = 4 Hz, 2H), 2.91 (hept, *J* = 6.7 Hz, 1H), 2.17 (s, 3H), 1.27 (d, *J* = 8 Hz, 6H); ESI-MS (m/z): 460.23 $[M-Cl]^+$-HCl; UV-Vis {Acetonitrile, λ_{max} nm ($\varepsilon/10^{-4}$ M^{-1} cm^{-1})}: 210 (6.895), 305 (6.406), 348 (2.558).

2.6.6 [(benzene)Ru($\kappa^1_{(N)}$-L2)Cl_2] (6)

Color: Yellow; Yield: 78%; FT-IR (KBr, cm^{-1}): 3445 (υ_{O-H}), 1647 ($\upsilon_{C=O}$), 1585-1506 ($\upsilon_{C=N}$); ^{1}H NMR (400 MHz, DMSO-d_6): δ 12.37 (s, 1H, OH), 9.03 (s, 1H), 8.62 (d, *J* = 4 Hz, 1H), 8.25 (d, *J* = 8 Hz, 1H), 8.12 (d, *J* = 12 Hz, 1H), 7.85 (d, *J* = 16 Hz, 1H), 7.57 (d, *J* = 8 Hz, 2H), 7.51 (dd, *J* = 4, 4 Hz, 1H), 7.04-6.99 (m, 3H), 5.95 (s, 6H); ^{13}C NMR (100 MHz, DMSO-d_6): δ = 193.2, 161.7, 151.2, 150.5, 141.1, 136.4, 135.2, 130.9, 130.2, 128.2, 123.7, 120.7, 119.2, 117.7, 85.5; ESI-MS (m/z): 404.05 $[M-Cl]^+$-HCl; UV-Vis {Acetonitrile, λ_{max} nm ($\varepsilon/10^{-4}$ M^{-1} cm^{-1})}: 201 (7.565), 305 (5.061), 348 (2.005).

2.6.7 [Cp*Rh($\kappa^1_{(N)}$-L2)Cl_2] (7)

Color: Orange; Yield: 82%; FT-IR (KBr, cm^{-1}): 3435 (υ_{O-H}), 1647 ($\upsilon_{C=O}$), 1593-1489 ($\upsilon_{C=N}$); ^{1}H NMR (400 MHz, DMSO-d_6): δ 12.69 (s, 1H), 9.39 (s, 1H), 9.13 (s, 1H), 8.14 (d, *J* = 8 Hz, 1H), 8.03 (d, *J* = 8 Hz, 1H), 7.97 (d, *J* = 16 Hz, 2H), 7.87 (d, *J* = 16 Hz, 1H), 7.66 (t, *J* = 8 Hz, 1H), 7.57 (t, *J* = 8 Hz, 1H), 7.17 (d, *J* = 8 Hz, 1H), 7.10 (t, *J* = 8 Hz, 1H), 1.74 (s, 15H); UV-Vis {Acetonitrile, λ_{max} nm ($\varepsilon/10^{-4}$ M^{-1} cm^{-1})}: 208 (6.325), 306 (5.466), 348 (2.361).

2.6.8 [Cp*Ir($\kappa^1_{(N)}$-L2)Cl_2] (8)

Color: Yellow; Yield: 83%; FT-IR (KBr, cm^{-1}): 3433 (υ_{O-H}), 1647 ($\upsilon_{C=O}$), 1588-1491 ($\upsilon_{C=N}$); ^1H NMR (400 MHz, DMSO-d_6) δ 12.38 (s, 1H), 9.03 (s, 1H), 8.62 (d, J = 8 Hz, 1H), 8.37 (d, J = 8 Hz, 1H), 8.25 (d, J = 8 Hz, 1H), 8.16 (d, J = 16 Hz, 1H), 7.85 (d, J = 16 Hz, 1H), 7.58 (t, J = 8 Hz, 1H), 7.50 (dd, J = 4, 4 Hz, 1H), 7.03 – 7.00 (m, 2H), 1.62 (s, 15H); ^{13}C NMR (100 MHz, DMSO-d_6 + $CDCl_3$): δ = 193.19, 162.27, 150.96, 150.35, 141.19, 136.31, 135.15, 130.18, 123.70, 123.15, 118.90, 117.66, 91.96, 8.18; UV-Vis {Acetonitrile, λ_{max} nm ($\varepsilon/10^{-4}M^{-1}$ cm^{-1})}: 210 (6.088), 305 (6.088), 348 (2.683).

3. Results and Discussion

3.1 Synthesis of complexes

In the present work, we have carried out the synthesis and biological activity evaluation of metal complexes of ruthenium, rhodium and iridium bearing pyridyl chalcone derivatives. Pyridyl chalcone derivatives (Scheme 1) were obtained following the procedure reported in the literature [22]. Treatment of [(arene)Ru(μ-Cl)Cl]$_2$, (arene = benzene, p-cymene), [Cp*M(μ-Cl)Cl]$_2$ (M=Rh and Ir) with ligand (**L1** or **L2**) in 1:2 (M:L) ratio has yielded a series of neutral monodentate mononuclear complexes **1-8** with the chemical formula [(arene)M{$\kappa^1_{(N)}$L1/L2}Cl_2]. Despite having extra binding sites of ligands towards metal, these ligands bind exclusively through pyridyl nitrogen. Ruthenium and iridium complexes are yellow in color while rhodium complexes are orange in color. These complexes are stable in the air as well as in solution and they are soluble in MeOH and partially soluble in dichloromethane, chloroform and acetonitrile and insoluble in solvents like hexane, diethyl ether and petroleum ether. The analytical data of these compounds are consistent with the formulations. All complexes were fully characterized by ^1H NMR, ^{13}C NMR, IR, CHN and Mass spectroscopy. The molecular structure of the complexes determined by single-crystal X-ray diffraction method, revealed the coordination of the metals to the ligands (**L1** and **L2**) only through the pyridyl nitrogen atom.

3.2 Spectral Studies of complexes (1-8)

3.2.1 Infrared Spectra (IR) of ligands and complexes

Information on the nature of the functional group attached to the metal atom was obtained using IR spectroscopy. The ligand **L1** IR spectrum displayed two bands at 3413 and 3284 cm^{-1} for the NH_2 group while ligand **L2** displayed one broadband at 3447 cm^{-1} for the OH group. Both the carbonyl group of the ligands displayed a strong band at around 1648-1653 cm^{-1}. All the complexes exhibited characteristic bands corresponding to C=N, C=O, C=C, OH and NH_2

stretching frequencies. The NH_2 frequencies were observed in the range of 3150-3480 cm^{-1}. The C=N and C=C bond vibrated at a higher frequency region as compared to the free ligand around 1583-1616 cm^{-1} and 1450-1546 cm^{-1} indicating the coordination of the metals to the ligands through the pyridine ring.

3.2.2 ^{1}H-NMR spectra of complexes

The ^{1}H-NMR spectra of the complexes displayed signals associated with the ligand protons and signals due to *p*-cymene and Cp* ring protons. The ^{1}H NMR spectra of the ligand **L1** displayed one singlet at 9.40 ppm assigned to the CH proton of the pyridine ring, the NH_2 proton signals were not observed due to solvent exchange with DMSO-d_6, the trans-CH protons with J = 16 Hz coupling constant were observed as a doublet at 7.68 and 8.26 ppm respectively and the aromatic protons of the ligand **L1** were observed in the downfield region around 6.55-8.96 ppm. The ^{1}H NMR spectra of the ligand **L2** displayed one singlet at 12.68 ppm assigned to the OH proton, a singlet at 8.89 ppm assigned to the CH proton of the pyridine ring, the trans-CH protons with J = 16 Hz coupling constant were observed at 7.73 and 7.90 ppm respectively and the aromatic protons of the ligand **L2** were observed in the downfield region around 6.95-8.89 ppm. To further reveal the coordination behavior of these ligands to metals and the formation of complexes, ^{1}H NMR analyses of all these complexes were recorded in deuterated DMSO-d_6 solvent at room temperature. The ligand aromatic protons of complexes **1**-**8** displayed the same splitting pattern with a slight shift of proton signals towards the downfield or upfield region which resulted from coordination of the metals to the ligand. The binding of the pyridyl chalcone ligand to the ruthenium atom for complex **1** and **5** was confirmed by the distinct splitting of the *p*-cymene ring protons upon coordination of the ligand to the *p*-cymene moiety. The signals associated with the *p*-cymene ligand consisted of two doublets around 5.86-5.91 ppm for the ring protons, one singlet at 2.17 ppm for the methyl protons and one doublet at 1.27 ppm for the isopropyl group. Also, the methine proton of the *p*-cymene group exhibited septet at around 2.86-2.96 ppm. Ruthenium benzene complexes **2** and **6** displayed one singlet at 5.95 assigned to the CH protons of the benzene ring. Rhodium and iridium complexes **3**, **4**, **7** and **8** bearing Cp* analog displayed one singlet in the range of 1.40-1.74 ppm. The NH_2 proton signals of the complexes **1**-**4** were not observed due to solvent interaction with DMSO-d_6 whereas the OH proton signals of complexes **5**-**8** were observed in the range of 12.37-12.69 ppm. The ^{1}H NMR of all these complexes were given in supplementary data (Figure S1 to S10).

3.2.3 *^{13}C-NMR spectra of complexes*

The ^{13}C-NMR spectra of the complexes further confirmed the formation and coordination of the metals to the ligands. The ^{13}C-NMR spectra of the complexes displayed signals associated with the carbon of the ligands, the *p*-cymene moiety, and the Cp* group. The aromatic signals for the ligand part of the complexes were observed in the range of 114.5-162.4 ppm. The carbonyl group carbon of the complexes displayed a signal around 189.6-198.7 ppm. The ring carbons of the *p*-cymene moiety displayed signals around 82.9-106.8 ppm whereas the methyl, methine and isopropyl carbons signals were observed around 17.8-29.9 ppm. The benzene ring carbons of the ruthenium benzene complexes displayed signals around 87.5-87.5 ppm. The Cp* methyl carbons signal was observed around 8.1 ppm and the Cp* ring carbons signal was observed at 91.9-92.1 ppm. These data are in good agreement with the previously reported complexes done by our group [23] thus supporting the formation of the complexes. The ^{13}C-NMR spectra of some of the complexes were given in supplementary data (Figure S11 to S14).

3.2.4 *Mass spectra of complexes*

The mass spectra of the complexes further confirmed the formation of metal complexes. The mass spectra of all the complexes except for complex **2** exhibited their predominant molecular ion peaks at m/z value, which corresponds to $[M\text{-}Cl]^+$-HCl ion peak. For instance, the mass spectrum of complexes **1** displayed its predominant molecular ion peak at m/z: 459.21, similarly for complexes **3**, **4**, **5** and **6** displayed their predominant molecular ion peak at m/z: 461.24, 551.30, 460.23 and 404.05 respectively which corresponds to $[M\text{-}Cl]^+$-HCl ion peak. In complex **2** the molecular ion peak was observed at m/z: 224.93, which is due to $[M\text{-}Cl]^+$-HCl-Ru-benzene ion peak. The mass ion peaks observed in these complexes are in accordance with similar reported complexes [23]. The mass spectra of some of the complexes were given in supplementary data (Figure S19 to S24).

3.2.5 *UV-visible spectra of complexes*

The electronic spectra of the monodentate mononuclear pyridyl chalcone complexes were recorded in acetonitrile at 10^{-4} M concentration at room temperature and the respective plots are shown in (Figure S25). The electronic spectra of the mononuclear complexes display two absorption bands in the higher energy region around 230-240 nm which can be assigned as ligand centered or intra ligand π-π* and low energy band at 290-305 nm corresponding to n-π* transition [24, 25]. Medium intensity band at 340-410 nm were also observed corresponding to

metal to ligand charge transfer where from Ru (4d) orbitals to the low-lying empty orbitals π* orbitals of the ligand. The low spin Rh(III) and Ir(III) complexes provide filled dπ (t_{2g}) orbitals which can interact with low lying π* orbitals of the pyridyl chalcone ligands and therefore we can expect a band attributable to metal to ligand charge transfer MLCT band.

3.3. Description of the molecular structures of complexes

The solid-state structures of some of the mononuclear complexes were established by single-crystal X-ray crystallography. The ORTEP view of the complexes along with the atom numbering scheme is shown in Figure 1. The summary of the crystal data, data collection and structure refinement parameters are summarized in Table S1. Selected bond lengths, bond angles and metal atom involving ring centroid values are listed in Table S2.

Single crystal analyses for the complexes were carried out to have a deeper understanding of the geometry of the complexes. By carrying out single-crystal analyses of the complexes we were able to confirm the bonding modes associated with the ligand. Single crystals suitable for X-ray diffraction analysis were obtained for complexes **2**, **4**, **5** and **7.** These crystals are yellow, orange and red in color and were obtained by the solvent diffusion method for all the complexes. In all the complexes with both ligands, the preferable mode of coordination of the metal is through pyridine nitrogen of the pyridyl chalcone forming monodentate mononuclear complexes. All these half-sandwich complexes adopt a typical three-legged "piano-stool" geometry in which the metal center is coordinated through one nitrogen donor atoms from the pyridine ring of the ligand and two terminal chloride which represents the three-leg of a piano while the arene ring (arene = *p*-cymene, benzene, Cp*) represent the seat of a piano. The molecular structure of these mononuclear complexes strongly supports the formation of these complexes and the coordination of ligands that occur through the pyridine nitrogen N(1) forming monodentate complexes (Figure 1). Complexes **2**, **4** and **7** crystallizes in monoclinic system with $P2_1/n$ and *Cc* space group while complex **5** crystallizes in a triclinic system with $P\bar{1}$ space group. The distance between the metal to the centroid of the *p*-cymene/Cp* ring of complexes **2**, **4**, **5** and **7** is 1.657 Å, 1.779 Å, 1.667 Å and 1.783 Å respectively. The M(1)-N(1) bond distances in these mononuclear complexes are in the range of 2.116-2.146 Å. The M(1)-Cl(1) bond distances for complexes **2**, **4** and **7** are in the range of 2.410-2.4170 Å while that of complex **5** were found to be slightly longer at 2.4320(19) Å. The M(1)-Cl(2) bond distances for complexes **2**, **4** and **7** are in the range of 2.4167-2.439 Å while that of complex **5** were found to be slightly shorter at 2.402(2) Å. These data are consistent

with the previously reported complexes of pyridyl-base ligands [26, 27]. The carbonyl (C=O) bond distances for complexes **2**, **4** and **7** are in the range of 1.228-1.247 Å, whereas complex **5** carbonyl bond distance is found to be slightly longer at 1.370(13) Å. The bond angle values Cl(1)-M(1)-Cl(2) of these complexes are in the range of 86.99°-91.65° and the Cl(1)-M(1)-N(1) and Cl(2)-M(1)-N(1) bond angle is also found to be in the range of 85.44°-88.22° which are consistent with the piano stool arrangement of various groups about the metal center and is comparable to previously reported values [26, 28].

3.4. Non-covalent interaction

From the crystal packing of some of the complexes, it was observed that complex (**2**) possessed intramolecular hydrogen bonding N-H·····O with 2.024 Å bond distance and 134.38° bond angle. Non-covalent interaction C-H·····Cl with 2.774 Å bond distance and 143.76° was observed between the CH group from the trans-CH=CH of ligand and chloride atom (Figure 2). Interestingly the crystal packing in complex (**2**) formed a dimeric unit *via* π-π stacking (3.582 Å) interaction known as supramolecular interaction. Complex **4**, on the other hand, possessed intramolecular hydrogen bonding N-H·····O with 2.010 Å bond distance and 128.93º bond angle and intermolecular hydrogen bonding C-H·····Cl with 2.766 Å bond distance and 140.66º bond angle. C-H····· π interaction involving the methyl C-H of the cp* ring and the phenyl ring of the ligand was also observed H_3C·····H (4.861 Å) (Figure 3). Further, the crystal structure of complex (**5**) crystallized with one CH_3OH molecule which formed one intramolecular hydrogen bonding O-H·····O with 1.804 Å bond distance and 146.61º bond angle and four different types of non-covalent C-H·····Cl (2.852, 2.931, 2.613 and 2.884 Å) interactions between chloride of the metal center and hydrogen atom from ligand and methanol molecule (Figure 4). Apart from these interactions complex **5** displayed interaction between the solvent of crystallization (CH_3OH) oxygen and the hydrogen from the pyridine ring of the ligand forming inter hydrogen bonding O·····H (2.613 Å).

3.5. Cytotoxicity studies against cancer cell lines

The response of cell lines to complexes **1-8**, ligands **1-2** and cisplatin are presented in Figure 5. Complexes **6-8** were inactive against all four cell lines at the highest dose tested (100 μM) whereas complex **5** and ligand **2** were moderately toxic to cells. In both cases, the activity of complex 5 and ligand **2** was greater against ARPE-19 non-cancer cells (except for HCT-116 $p53^{-/-}$ cells treated with ligand **2**). This is reflected in the poor selectivity indices presented in Figure

6. In sharp contrast, ligand **L1** and complexes **1-4** were potent cytotoxic agents with comparable IC_{50} values to cisplatin. Except for complex **1**, complexes **2-4** and ligand **1** showed comparable or enhanced selectivity for cancer as opposed to non-cancer cells. Of particular interest is the observation that HCT-116 $p53^{-/-}$ cells are less responsive to cisplatin than HCT-116 with wild type p53 (Figure 5). In contrast, complexes **2-4** remain active against HCT-116 cells with defective p53 and consequently retain their good selectivity index for these cancer cells compared to ARPE-19 cells (Figure 6). As colorectal tumors with mutant or dysfunctional p53 are widely regarded as chemotherapy-resistant more aggressive cancers [29] this observation is potentially significant and worthy of further investigation. In general the tested compounds for anticancer activity against HCT-116 $p53^{+/+}$, HCT-116 $p53^{-/-}$ and HT-29 human colorectal cancer cell lines and were found that ligand **L1** and its complexes **1-4** show excellent activity. Ligand **L2** and complex **5** displayed moderate activity whereas complexes **6-8** lacked activity even at a higher dose (>100 μM). Furthermore, ligand **L1** and complexes **2**, **3** and **4** displayed a level selectivity comparable to cisplatin. Mai et al. reported chalcone derivatives containing $-NH_2$ group on ring A and phenyl group on ring B showed better cytotoxicity activity with IC_{50} = 4.39μM against HT-29 cancer cell [11]. However, in this work when ring A of chalcone derivatives contain $-NH_2$ group and ring B is replaced with pyridyl substituent an improved cytotoxicity activity with IC_{50} = 2.10μM against HT-29 cancer cell was observed which is even better than that of cisplatin. Hence, we can conclude that a slight change in the structure of the compound can have a significant effect on the activities of the whole ligand and complexes. Also, ligand **L1** and ligand **L2** differ only at ring A with R= NH_2 for **L1** and R= OH for **L2** whereas the activity of **L1** is 5 to 10 times more than that of **L2**.

3.6. In vitro antimicrobial activity of complexes and ligands

The synthesized ligands and complexes were evaluated for their *in-vitro* antibacterial activity against gram-positive; *Staphylococcus aureus* and gram-negative; *Escherichia coli*, *Klebsiella pneumoniae* strains by using standard techniques. The zones of inhibition (mm) in comparison with ciprofloxacin were given in Table (3) and the chart representation was given in Figure 7. All the compounds exhibited potent antibacterial activity against the tested organisms. *In-vitro* assay results revealed that complex **5** (17 ± 0.58 mm) and complex **7** (16 ± 0.56 mm) have better activity against gram-positive (*Staphylococcus aureus*). Complex **5** (17 ± 0.62 mm) and complex **7** (16 ± 0.68 mm) also showed highest activity against gram-negative (*Escherichia*

coli) while complex **5** (16 ± 0.45 mm) and complex **7** (15 ± 0.35 mm) showed moderate activity against gram-negative (*Klebsiella pneumoniae*).

The minimum inhibitory concentration (MIC) and minimum bactericidal concentration (MBC) results were listed in Table 4 and their chart representation was given in Figure 8. The MIC & MBC values of the compounds ranged from 0.125 to 1.0 mg/mL against all three organisms. Complex **3** and complex **7** values ranged from 0.125 to 0.25 mg/mL for *S. aureus*, *E. coli* and *Klebsiella pneumoniae*. The MIC & MBC values of ciprofloxacin ranging from 0.031 to 0.062 mg/mL and 0.062 to 0.0125 mg/mL against the tested organisms were taken as standard.

4. Conclusion:

All together eight new complexes have been synthesized. All the complexes were isolated as neutral compounds. The ligands and complexes were obtained in good yields and were characterized by analytical and spectral methods. Single crystal X-ray diffraction study reveals that the pyridyl chalcone ligands coordinated to the metal center only through the nitrogen atom of the pyridine ring forming neutral monodentate complexes. Cytotoxicity studies against cancer (HCT-116 $p53^{+/+}$, HCT-116 $p53^{-/-}$ and HT-29 human colorectal cancer cells) and non-cancer (ARPE-19 retinal epithelium) cells demonstrated that ligand **L1** and its associated complexes were more active compared to ligand **L2** and its associated complexes**.** Furthermore, the increased potency is accompanied by a significant increase in selectivity, particularly with regards to HCT-116 cells with defective p53. Whilst potency and selectivity were comparable to cisplatin, the fact that complexes 2-4 retained activity against HCT-116 $p53^{-/-}$ cells marks these compounds as having different properties to cisplatin. Anti-bacterial studies for all the compounds have also been carried out and they were found to be active against all the three bacterial strains.

5. Acknowledgment

Lincoln Dkhar thanks SAIF-NEHU for spectral analyses and DST-PURSE SCXRD, India for providing Single Crystal X-ray analysis. Lincoln Dkhar also thank the Department of Science and Technology (DST), India for providing financial assistance under the Innovation in Science Pursuit for Inspired Research (INSPIRE) fellowship.

6. Supplementary Material

CCDC 1908852 (**2**), 1908853 (**3**), 1908854 (**5**) and 1908855 (**7**) contains the supplementary crystallographic data for this paper. These data can be obtained free of charge via www.ccdc.cam.ac.uk/data_request/cif, by e-mailing data_request@ccdc.cam.ac.uk, or by contacting The Cambridge Crystallographic Data Centre, 12, Union Road, Cambridge CB2 1EZ, UK; Fax: +44 1223 336033.

7. References

[1] D.R. Williams, Chem. Rev., 72 (1972) 203–213.

[2] (a) A. Casini, C.G. Hartinger, A.A. Nazarov, P.J. Dyson, Top. Organomet. Chem., 32 (2010) 57. (b) P.J. Dyson, G. Sava, Dalton Trans., (2006) 1929. (c) A. Peacock, P.J. Sadler, Chem. Asian J., 3 (2008) 1890. (d) L. Ronconi, P.J. Sadler, Coord. Chem. Rev., 251 (2007) 1633. (e) C.G. Hartinger, A.D. Phillips, A. Nazarov, Curr. Top. Med. Chem., 11 (2011) 2688. (f) C. Mu, S.W. Chang, K.E. Prosser, A.W.Y. Leung, S. Santacruz, T. Jang, J.R. Thompson, D.T.T. Yapp, J.J. Warren, M.B. Bally, T.V. Beischlag, C.J. Walsby, Inorg. Chem., 55 (2016) 177. (g) G.S. Smith, B. Therrien, Dalton Trans., 40 (2011) 10793.

[3] P. Zhang, P.J. Sadler, J Organomet Chem., 839 (2017) 5.

[4] (a) C.G. Hartinger, P.J. Dyson, Chem. Soc. Rev., 38 (2009) 391. (b) G. Gasser, I. Ott, N.J. Metzler-Nolte, Med. Chem., 54 (2011) 3. (c) A.F.A. Peacock, A. Habtemariam, R. Fernandez, V. Wall, F.P.A. Fabbiani, S. Parsons, R.E. Aird, D.I. Jodrell, P.J. Sadler, J. Am. Chem. Soc., 128 (2006) 1739. (d) R. Schuecker, R.O. John, M.A. Jakupec, V.B. Arion, B.K. Keppler, Organometallics., 27 (2008) 6587. (e) I. Romero-Canelon, P.J. Sadler, Inorg. Chem., 52 (2013) 12276.

[5] (a) G. Suss-Fink, Dalton Trans., 39 (2010) 1673. (b) C.S. Allardyce, P.J. Dyson, Platinum Met. Rev., 45 (2001) 62. (c) M.J. Clarke, Coord. Chem. Rev., 236 (2003) 209. (d) B.T. Loughrey, P.C. Healy, P.G. Parsons, M.L. Williams, Inorg. Chem., 47 (2008) 8589–8591.

[6] H.K. Liu, P.J. Sadler, Acc. Chem. Res., 44 (2011) 349.

[7] (a) R.E. Morris, R.E. Aird, P.D. S. Murdoch, H. Chen, J. Cummings, N.D. Hughes, S. Parsons, A. Parkin, G. Boyd, D.L. Jodrell, P.J. Sadler, J. Med. Chem., 44 (2001) 3616.

(b) O. Novakova, H. Chen, O. Vrana, A. Rodger, P.J. Sadler, V. Brabec, Biochemistry., 42 (2003) 11544.

[8] A. Kurzwernhart, W. Kandioller, S. Bachler, C. Bartel, S. Martic, M. Buczkowska, G. Muhlgassner, M.A. Jakupec, H. B. Kraatz, P.J. Bednarski, V.B. Arion, D. Marko, B.K. Keppler, C.G. J. Hartinger, J Med Chem., 55 (2012) 10512−10522.

[9] J. Pitchaimani, M.R.C. Raja, S. Sujatha, S.K. Mahapatra, D. Moon, S.P. Anthony, V. Madhu, RSC Adv., 6 (2016) 90982.

[10] M. Saleh, S. Abbott, V. Perron, C. Lauzon, C. Penney, B. Zacharie, Bioorg Med Chem Lett., 20 (2010) 945-949.

[11] C.W. Mai, M. Yaeghoobi, N.A. Rahman, Y.B. Kang, M.R. Pichika, Eur. J. Med. Chem., 77 (2014) 378.

[12] Crysalis P R O, release 2012 Version 1.171.36.20. Agilent Technologies, Yarnton.

[13] G.M. Sheldrick, (1997) SHELXL-97, Program for the Refinement of Crystal Structures. University of Göttingen, Germany.

[14] G.M. Sheldrick, Acta Crystallogr., (2015) C71 3.

[15] L.J. Farrugia, J. Appl. Crystallogr., 30 (1997) 565.

[16] L.J. Farrugia, J. Appl. Crystallogr., 32 (1999) 837.

[17] F. Bunz, A. Dutriaux, C. Lengauer, T. Waldman, S. Zhou, J. P. Brown, J. M. Sedivy, K. W. Kinzler, B. Vogelstein, Science., 282 (1998) 497–1501.

[18] S.J. Lucas, R.M. Lord, R.L. Wilson, R.M. Phillips, V. Sridharan, P.C. McGowan, Dalton Trans., 2012, 41, 13800.

[19] Z. Almodares, S.J. Lucas, B.D. Crossley, A.M. Basri, C.M. Pask, A.J. Hebden, R.M. Phillips, P.C. McGowan, Inorg. Chem., 53 (2014) 727.

[20] B. Venkanna, A. Uma, Ch. Suvarnalaxmi, N. Chandrasekharnath, R.S. Prakasham, L. Jayalaxmi, Curr. Trends Biotechnol. Pharm., 7 (2013) 782-792.

[21] V. Banothu, C. Neelagiri, A. Adepally, J. Lingam, K. Bommareddy, Pharm Biol., 55 (2017) 1155-1161.

[22] (a) A. Nie, J. Wang, Z.J. Huang, Comb. Chem., 8 (2006) 646-648. (b) N. Punna, K. Harada, J. Zhou, N. Shibata, Org. Lett., 21 (2019) 1515-1520. (c) A.F.C. Ortiz, A.S. Lopez, A.G. Rıos, F.C. Cabezas, C.E.R. Correa, J. Mol. Struct., 216 (2015) 1098.

[23] S. Adhikari, O. Hussain, R.M. Phillips, W. Kaminsky, M.R. Kollipara, Appl. Organomet. Chem. 32 (2018) 4362.

[24] P. Didier, I. Ortmans, A. Kirsch- De Mesmaeker, R. Watts, Inorg. Chem., 32 (1993) 5239-5245.

[25] B. Sullivan, D. Salmon, T. Meyer, Inorg. Chem., 17 (1978) 3334- 3341.

[26] C.M. Clavel, E. Paunescu, P. Nowak-Sliwinska, A.W. Griffioen, R. Scopelliti, P.J. Dyson, J. Med. Chem., 2015, 58, 3356− 3365.

[27] C.M. Clavel, E. Paunescu, P. Nowak-Sliwinska, A.W. Griffioen, R. Scopelliti, P.J. Dyson, J. Med. Chem., 2014, 57, 3546−3558.

[28] S. Adhikari, W. Kaminsky, M.R. Kollipara, J. Organomet. Chem., 848 (2017) 95-103.

[29] X.-L. Li, J. Zhou, Z.-R. Chen, W.-J. Chng, World J Gastroenterol., 21 (2015) 84–93.

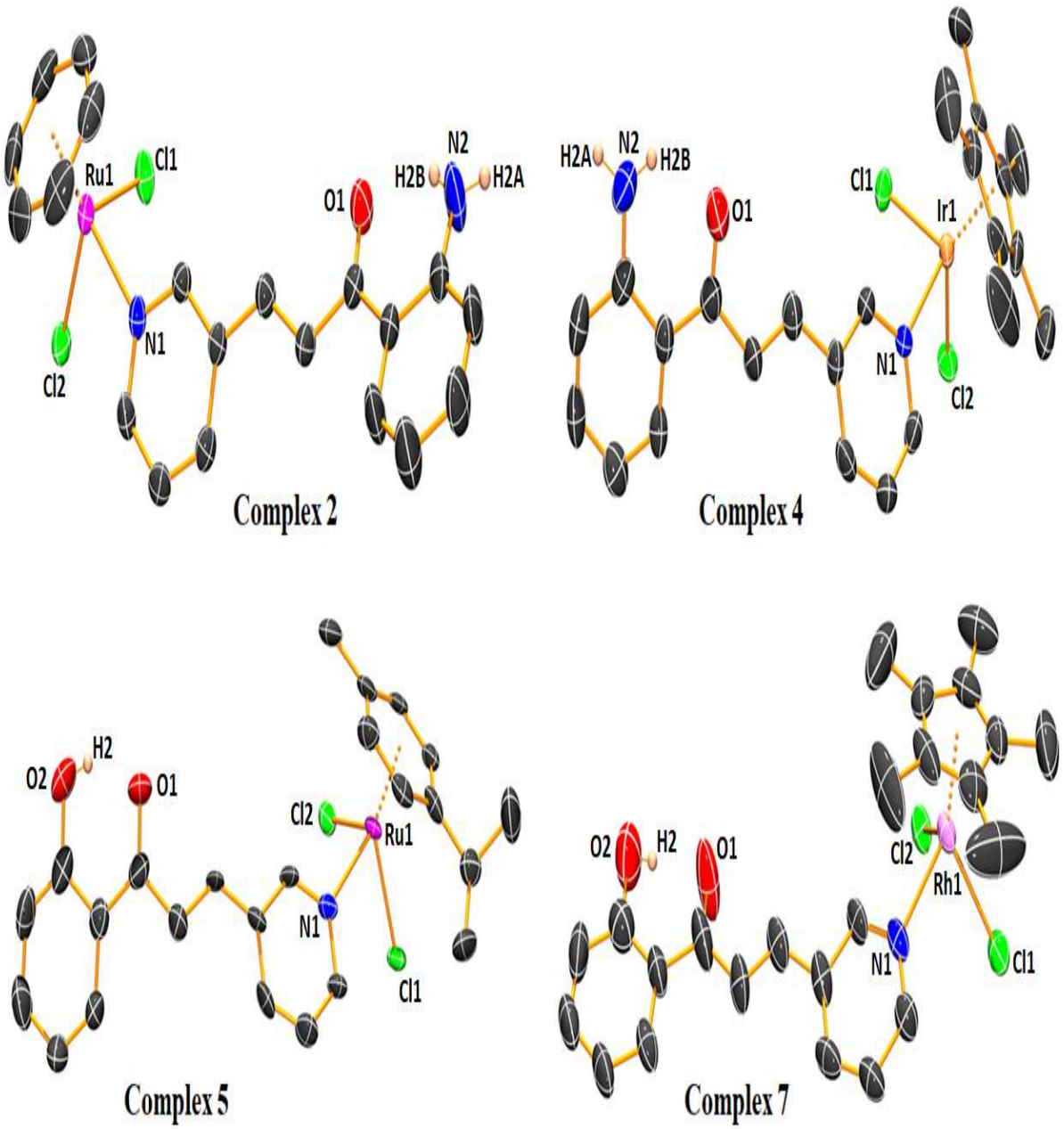

Figure 1: ORTEP generated molecular structure of complexes **2**, **4**, **5** and **7** with 50% thermal ellipsoid probability. Hydrogen atoms (except on N2 and O2) are omitted for clarity purpose.

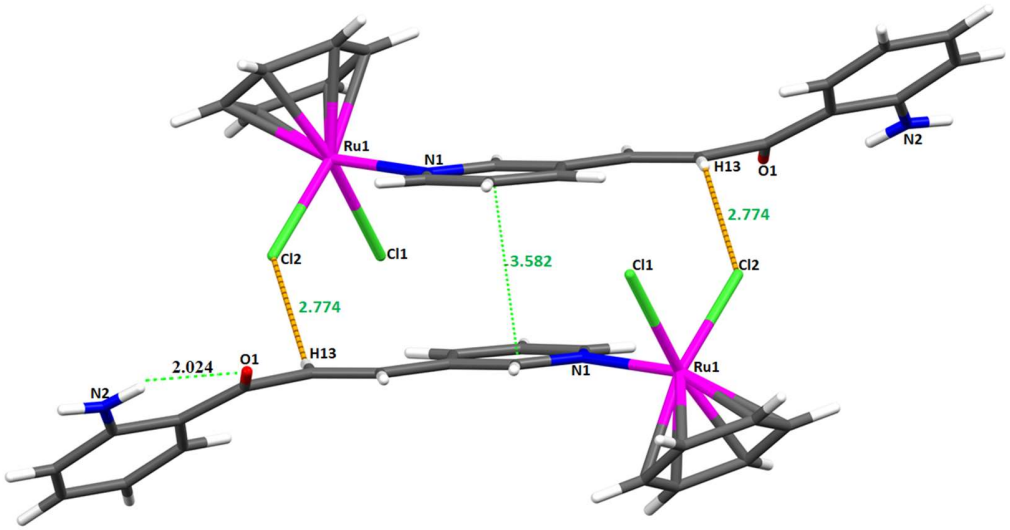

Figure 2: Crystal packing of complex **2** showing intramolecular and supramolecular interaction.

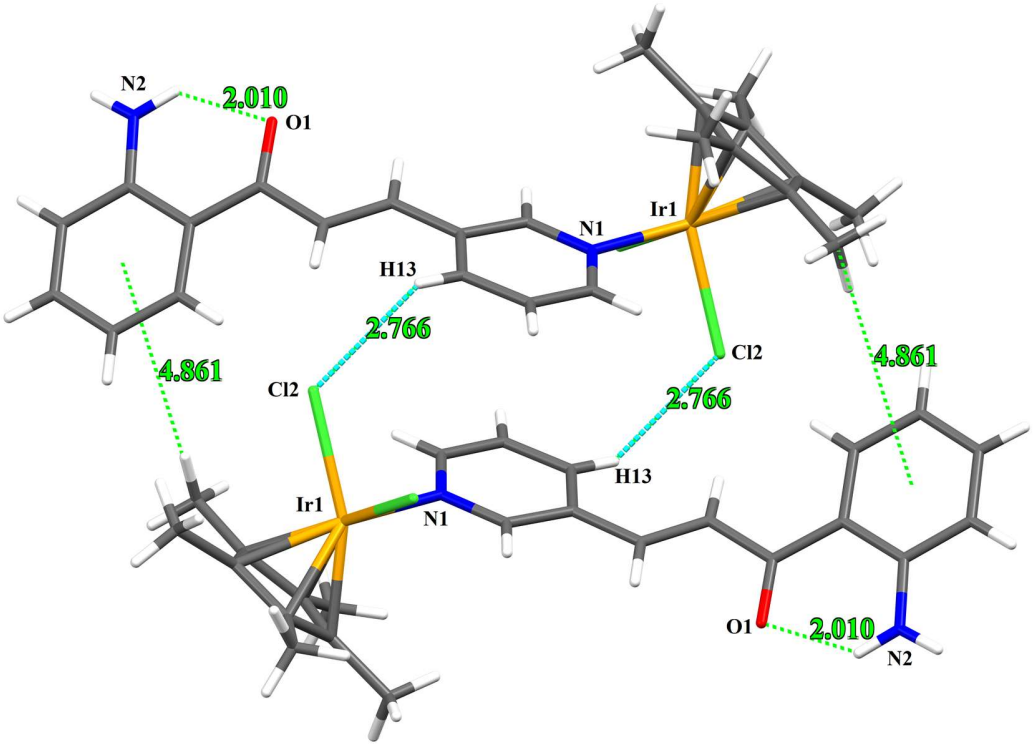

Figure 3: Crystal packing of complex **4** showing inter and intra molecular hydrogen bonding.

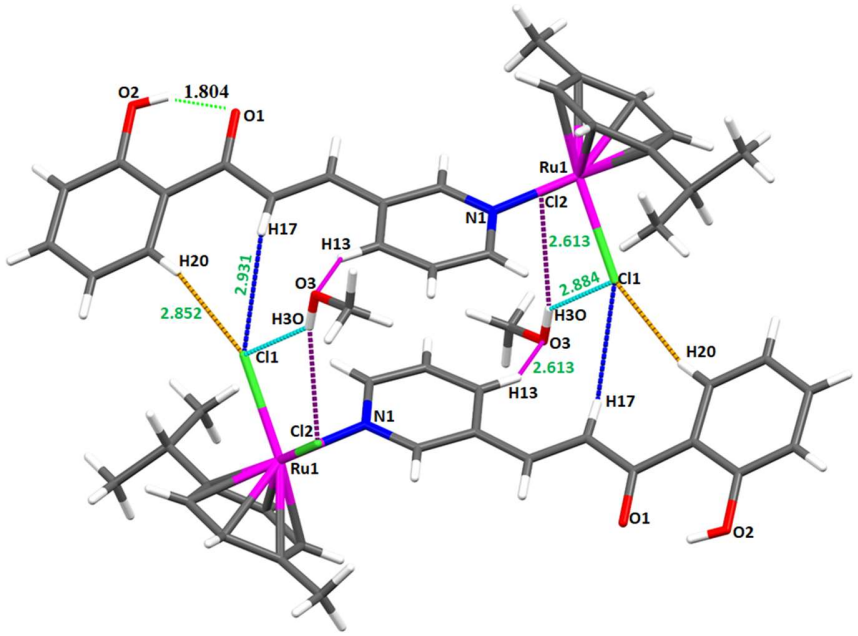

Figure 4: Crystal packing of complex **5** showing inter and intra molecular hydrogen bonding.

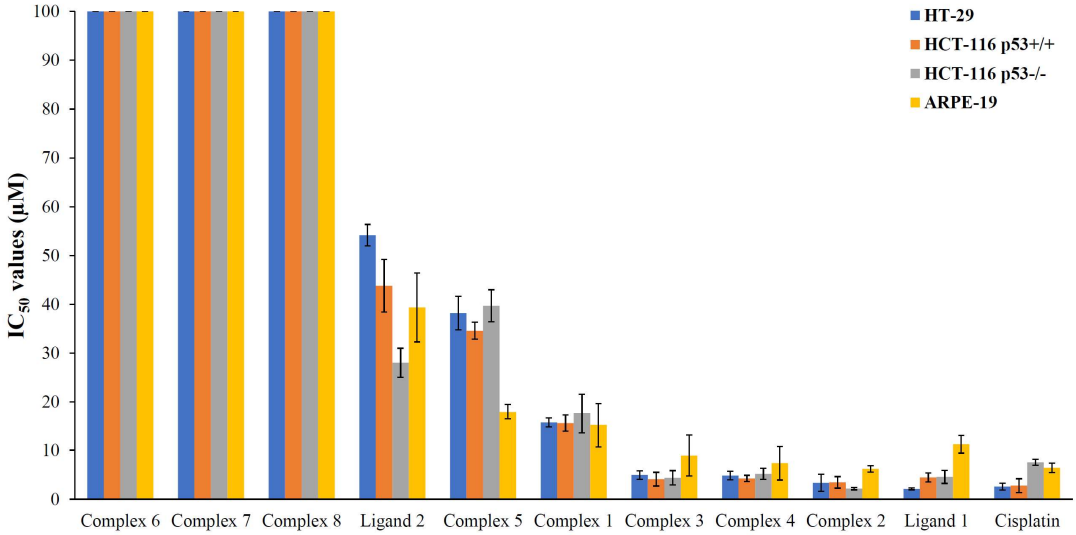

Figure 5: Response of a panel of cancer cells and ARPE-19 non-cancer cells following a continuous exposure (96 hours) to complex 1 to 8, ligands 1 to 2 and cisplatin. Each value represents the mean IC_{50} ± standard deviation for three independent experiments. Complex 6, 7 and 8 have IC_{50} values >100 µM which was the highest dose tested.

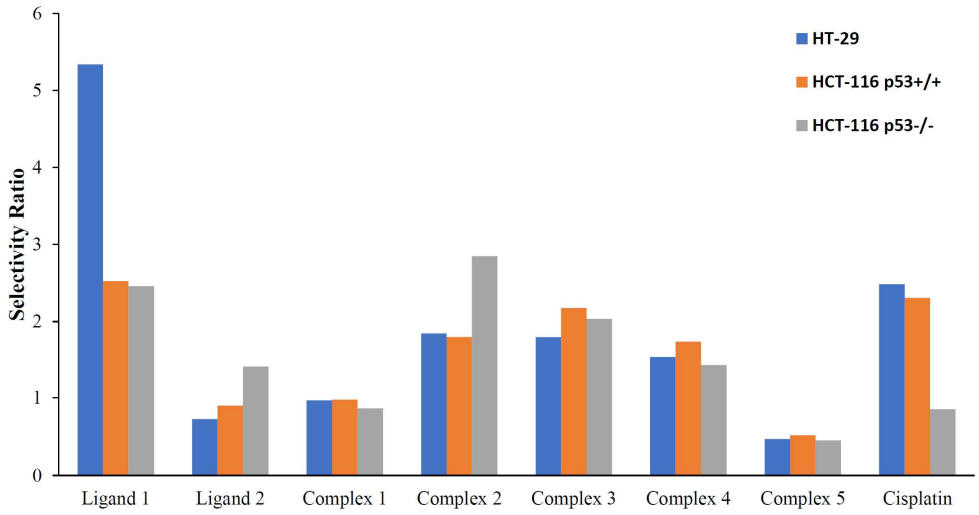

Figure 6: Selectivity ratios for complexes 1 to 5, ligands 1 and 2 and cisplatin. The selectivity ratio is defined as the ratio of IC_{50} values for ARPE-19 divided by the IC_{50} for each cancer cell line. Values greater than 1 (as indicated by the broken line) represent compounds that are preferentially active against cancer cells compared to non-cancer ARPE-19 cells. As the selectivity ratio is calculated using the mean IC_{50} values, no error bars are presented on this figure.

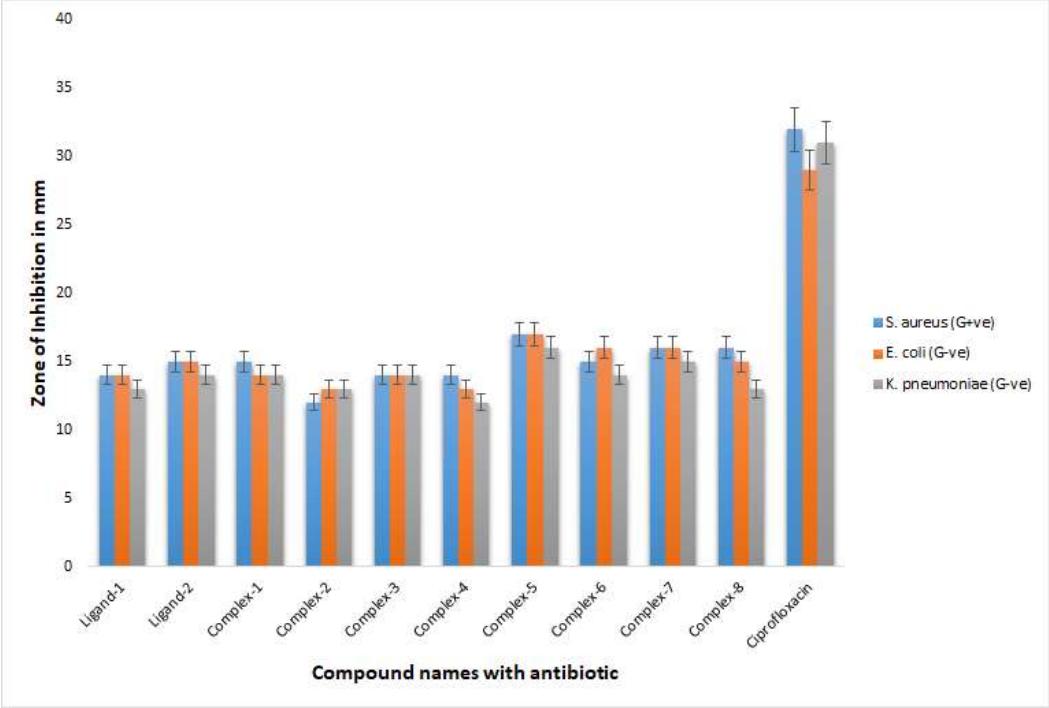

Figure 7: Figure showing antimicrobial activity (Agar well) of the studied compounds

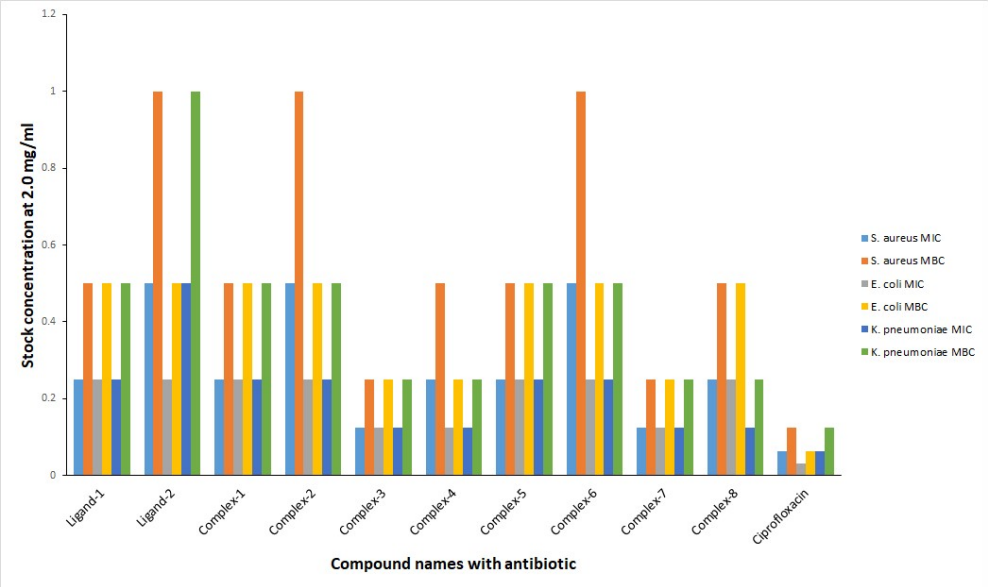

Figure 8: Figure showing MIB and MIC of tested compounds

Table 1: IC_{50} values of pyridyl chalcone (**L1** and **L2**) and complexes **1-8** along with cisplatin against HT-29, HCT-116 $p53^{+/+}$, HCT-116 $p53^{-/-}$ cancer cell lines and non-cancer cell line ARPE-19. Each value represents the mean ± standard deviation from three independent experiments.

Compounds	**IC_{50} (µM)**			
	HT-29	**HCT-116 $p53^{+/+}$**	**HCT-116 $p53^{-/-}$**	**ARPE-19**
Ligand 1	2.10 (+/- 0.19)	4.44 (+/- 0.91)	4.56 (+/- 1.35)	11.21 (+/- 1.82)
Ligand 2	54.18 (+/- 2.19)	43.83 (+/- 5.39)	28.06 (+/- 2.95)	39.39 (+/- 7.05)
Complex 1	15.64 (+/- 0.88)	15.51 (+/- 1.64)	17.56 (+/- 4.04)	15.15 (+/- 4.49)
Complex 2	3.35 (+/- 1.73)	3.44 (+/- 1.17)	2.17 (+/- 0.26)	6.18 (+/- 0.68)
Complex 3	4.95 (+/- 0.86)	4.09 (+/- 1.38)	4.37 (+/- 1.45)	8.89 (+/- 4.18)
Complex 4	4.82 (+/- 0.85)	4.23 (+/- 0.64)	5.17 (+/- 1.13)	7.35 (+/- 3.42)
Complex 5	38.21 (+/- 3.42)	34.60 (+/- 1.73)	39.72 (+/- 3.28)	17.96 (+/- 1.55)
Complex 6	>100	>100	>100	>100
Complex 7	>100	>100	>100	>100
Complex 8	>100	>100	>100	>100
Cisplatin	2.58 (+/- 0.72)	2.78 (+/- 1.4)	7.52 (+/- 0.65)	6.41 (+/- 0.95)

NB - values at 100 = >100 indicates no IC50 at the highest dose tested on 100 µM

Table 2: Selectivity ratios of ligands and complexes along with cisplatin in HT-29, HCT-116 $p53^{+/+}$, HCT-116 $p53^{-/-}$ cancer cell lines.

Compounds	Selectivity Ratio (HT-29)	Selectivity Ratio (HCT-116 $p53^{+/+}$)	Selectivity Ratio (HCT-116 $p53^{+/+}$)
Ligand 1	5.338	2.525	2.458
Ligand 2	0.727	0.899	1.404
Complex 1	0.969	0.977	0.863
Complex 2	1.845	1.797	2.848
Complex 3	1.796	2.174	2.034
Complex 4	1.525	1.738	1.422
Complex 5	0.470	0.519	0.452
Cisplatin	2.484	2.306	0.852

Table 3: Antibacterial activity (Agar well) of tested compounds

S. No.	Compound Names	Zone of inhibition (Diameter in mm) at conc. 200 µg		
		S. aureus	***E. coli***	***K. pneumoniae***
1	Ligand-L1	14 ± 0.22	14 ± 0.18	13 ± 0.10
2	Ligand-L2	15 ± 0.35	15 ± 0.48	14 ± 0.15
3	Complex-1	15 ± 0.26	14 ± 0.16	14 ± 0.32
4	Complex-2	12 ± 0.12	13 ± 0.12	13 ± 0.23
5	Complex-3	14 ± 0.38	14 ± 0.24	14 ± 0.36
6	Complex-4	14 ± 0.26	13 ± 0.16	12 ± 0.08
7	Complex-5	17 ± 0.58	17 ± 0.62	16 ± 0.45
8	Complex-6	15 ± 0.35	16 ± 0.45	14 ± 0.22
9	Complex-7	16 ± 0.56	16 ± 0.68	15 ± 0.35
10	Complex-8	16 ± 0.29	15 ± 0.19	13 ± 0.15
11	Ciprofloxacin	32 ± 0.40	29 ± 0.10	31 ± 0.20

S. aureus = *Staphylococcus aureus*; *E. coli* = *Escherichia coli*; *K. pneumoniae* = *Klebsiella pneumoniae*, NI: No Inhibition and Data are means (n = 3) ± Standard deviation of three replicates.

Table 4: Antibacterial activity (MIC & MBC) of tested compounds

S. No.	Compound Names	Stock concentration in 2.0 mg/mL					
		S. aureus		***E. coli***		***K. pneumoniae***	
		MIC	**MBC**	**MIC**	**MBC**	**MIC**	**MBC**
1	Ligand-L1	0.25	0.5	0.25	0.5	0.25	0.5
2	Ligand-L2	0.5	1.0	0.25	0.5	0.5	1.0
3	Complex-1	0.25	0.5	0.25	0.5	0.25	0.5
4	Complex-2	0.5	1.0	0.25	0.5	0.25	0.5
5	Complex-3	0.125	0.25	0.125	0.25	0.125	0.25
6	Complex-4	0.25	0.5	0.125	0.25	0.125	0.25
7	Complex-5	0.25	0.5	0.25	0.5	0.25	0.5
8	Complex-6	0.5	1.0	0.25	0.5	0.25	0.5
9	Complex-7	0.125	0.25	0.125	0.25	0.125	0.25
10	Complex-8	0.25	0.5	0.25	0.5	0.125	0.25
11	Ciprofloxacin	0.062	0.125	0.031	0.062	0.062	0.125

S. aureus = Staphylococcus aureus; *E. coli = Escherichia coli*; *K. pneumoniae = Klebsiella pneumoniae*.